High-Speed Coplanar Transmission Lines

Ulrich D. Keil, Douglas R. Dykaar, *Member, IEEE*, A. F. J. Levi, Rose F. Kopf, L. N. Pfeiffer, Sheldon B. Darack, and K. W. West

***Abstract*—We present measurements of picosecond pulse propagation on coplanar strip transmission lines for which speed (i.e., group velocity), as well as phase and amplitude information are measured.**

Electrode effects are studied using transmission line loops 1 mm in diameter with cumulative propagation distances as long as 6 cm. The intrinsically low dielectric constant of coplanar-air transmission lines is shown to result in high signal speed and *low attenuation*. We use our data to verify the applicability of a model based largely on empirical formulae for radiation loss (geometry) and conductor absorption. The model is then used to identify optimal design criteria (for a given bandwidth) and is extended to the case of small dimensions.

I. Introduction

At present data rates in conventional high speed digital electronics are in the 20–40 Gbs^{-1} range [1]. It is interesting to speculate on what problems may be encountered at, say, ten times this data rate. Maintaining the fidelity of digital signals at very high data rates requires optimization of on chip transmission line designs. For example, a 400 Gbs^{-1} digital data rate, implies that the -3 dB bandwidth for the clock is around 600 GHz. The choice of an appropriate technique to distribute such high bandwidth signals on length scales of the order of a typical chip dimension (i.e., 1 cm) has been the subject of some discussion [2]. In this paper we consider the effects of substrate dielectric and electrode properties on transmission lines intended to operate in this regime. We show that propagation speed (i.e., group velocity, defined as the velocity of the peak of the pulse) is roughly independent of temperature, while reducing the dielectric constant results in *faster* propagation, *reduced* attenuation, and reduced line charging energies.

Recent publications of measured [3]–[5] as well as modeled [6] propagation of fast electrical transients on coplanar strip transmission (CPS) lines have not considered the aspect of velocity in signal propagation. Some delay measurements have been reported, [7], [8] but no study of the impact propagation *speed* has on the modeling of measured results. While it has been noted that a uniform dielectric minimizes radiation loss [7], [9], the influence of substrate dielectric on propagation speed has only recently been measured [10], [11].

Manuscript received February 28, 1992; revised June 2, 1992. The work of U.D. Keil was supported by the Deutsche Forschungsgemeinschaft.

The authors are with AT&T Bell Laboratories, Murray Hill, NJ 07974.

IEEE Log Number 9202452.

We report on propagation of picosecond electrical pulses over distances ≤ 6 cm using a large diameter (1 mm) loop transmission line. Use of a loop configuration allows precise velocity, as well as phase and amplitude measurements to be made, simultaneously. Measurements are made for both ordinary coplanar strip and etched coplanar-air transmission (CAT) lines for both loop and straight-line configurations. We consider the effects of substrate dielectric, conductor temperature and conductor thickness on attenuation and propagation speed. The results are modeled using a standard dispersion model [3] considering only the dominant mechanisms of radiation loss and conductor absorption.

II. Test Structures

Coplanar strip transmission lines are fabricated on low temperature grown (LT) GaAs photoconductors [12], [13]. Fig. 1(a) shows a schematic of the loop configuration used in this work. A cross-sectional view is shown in Fig. 1(b). The conductor dimensions are width, $w = 5$ μm with spacing, $s = 5$ μm. Electrode thickness varies from 0.24 to 1.23 μm of evaporated Au. Some samples are fabricated with additional ohmic layer (Ge/Pd, 50 nm) or adhesion layer (Ti, 15 nm) before evaporation of the Au conductor. Loops are either 0.5 or 1 mm in diameter. Voltage is applied through perpendicular 5 μm wide bias lines. Photoconductive (gapless [14] or sliding contact [15]) switches are formed wherever a short optical pulse illuminates the region between the electrodes. The laser pulses are generated at 100 MHz by a colliding pulse mode-locked laser producing sub 100 fs pulses at full width and half maximum (FWHM) with a wavelength of 620 nm [16]. Electrooptic techniques [17] are used to measure pulse shape at minimum propagation distance and thereby define the input pulse for numerical simulations. All electrical input pulses used in this paper are measured to be ≤ 1 ps FWHM.

CAT lines are formed by evaporating coplanar transmission lines on a 200 nm layer of SiO_2. The layer of SiO_2 acts both as an etch mask and as a physical cantilevered support for the lines as shown in an SEM micrograph in Fig. 2. Islands of unetched material form the photoconductive switches which are connected to the electrodes through openings in the SiO_2 layer. The electrodes overhang the SiO_2 layer by about 2 μm, so the region of high-

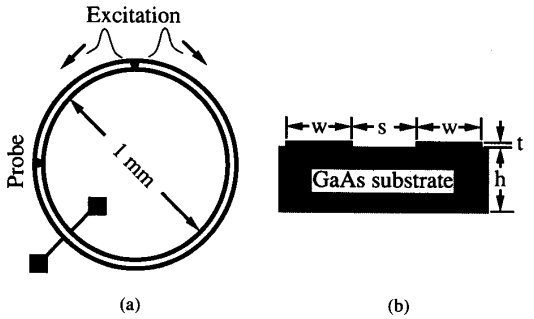

Fig. 1. (a) Loop configuration. The spots are shown for $\frac{1}{4}$ lap pump and probe sampling. Pulses are launched in both directions, resulting in sampling at the probe positions of signals having traveled $\frac{1}{4}$ and $\frac{3}{4}$ of a lap. For both beams located adjacent to bias lines, the lines act as a power splitter, preventing accurate amplitude measurements to be made. (b) Cross-sectional view.

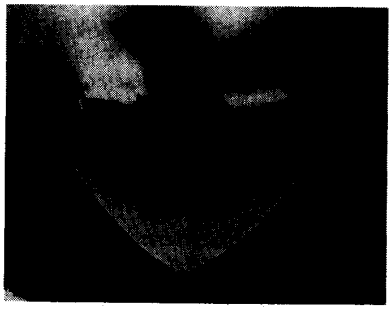

Fig. 2. Scanning electron micrograph of the etched CAT line. Linewidth and spacing is 5 μm. The SiO_2 layer extends about halfway underneath each electrode.

est field strength experiences a uniform air dielectric. This design has also been tested in a telephone pole type geometry where narrow strips of SiO_2 are fabricated perpendicular to the gold lines with 100 μm separations. All the etched designs are robust, not affected by wet processing or ultrasonic wire bonding. The etching process can be continued until electrical contact is lost between the metal lines and the photoconductive switch.

In a conventional electrooptic measurement, changing electrical propagation distance requires changing *both* the beam and $LiTaO_3$ sampling crystal positions for each value of propagation distance. Care must be taken so that only electrical propagation distance is changed, and not the optical propagation distance, which would introduce artifactual delays. Typically this requires the use of an optical fiber [10]. Here, pump and probe sampling [18] is used to generate and then sample the pulse as it travels around the loop. The optical beams are chopped at different frequencies and the signal is detected at the bias pads of the loop at the difference frequency (1.2 kHz) using a lock-in amplifier. This sampling technique eliminates the $LiTaO_3$ sampling crystal as a source of reflections and the loop eliminates the need to reposition the beams for each propagation distance, as the pulse comes back around the loop after completing each lap. In addition, the small size

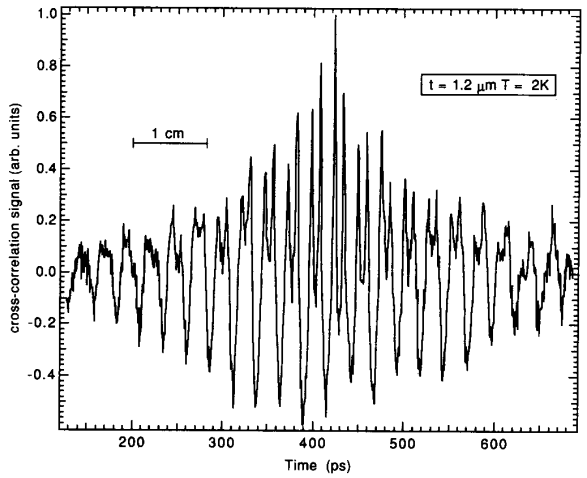

Fig. 3. Cross-correlation measurement on a CPS loop 1 mm diameter with pump and probe beams 0.5 mm apart. The line marked 1 cm indicates the propagation distance corresponding to the time scale. The sinusoidal background (few GHz) has been subtracted off (high-pass filtered).

of the loop allows measurements to be made in cryogenic environments where only narrow optical access is available.

By adjusting the spatial separation of the pump and probe beams any propagation distance can be defined. For example, $\frac{1}{4}$ loop (or lap) separation will result in sampling pulses that have propagated *both* $\frac{1}{4}$ and $\frac{3}{4}$ of a lap around the loop, as well as multiple laps, until the pulse decays completely. As shown in Fig. 1(a) the pulses are launched and travel around the loop in opposite directions to arrive at the sampling site. This geometry allows pulse propagation to be studied over much longer distances than previous measurements, while still maintaining absolute timing information (velocity) about the pulse. Fig. 3 shows a data trace for a 1 mm CPS loop at $T = 2\ K$ and 1.2 μm electrode thickness. The sinusoidal background is subtracted off (by high pass filtering the raw data) in all figures. The difference in pulse amplitude is due to the initial excitation launching pulses in opposite directions (i.e., different propagation distances for the two directions). As the beam delay goes from negative to positive delays, the role of the beams changes from pump and probe to probe and pump, i.e., causality requires that the first beam to arrive is the pump beam.

III. Theory

The calculation of attenuation and dispersion is carried out in the frequency domain. The signal propagation is described by

$$V(f, z) = V(f, 0)e^{-(\alpha(f) + j\beta(f))z} \quad (1)$$

where $V(f, z)$ is the Fourier transform of the signal pulse $v(t, z)$ at frequency, f and distance, z, $\alpha(f)$ is the frequency dependent attenuation constant and $\beta(f)$ the frequency dependent propagation constant. After propagation in the frequency domain the resultant signal is

recovered by performing an inverse Fourier transform. Only the dominant mechanisms of metal electrode absorption and radiation losses are considered here. As these measurements give sensitive information about the phase we will also review the contributions of the electrodes, and the dielectric to the phase term.

A. Velocity

For two half spaces of dielectric, ϵ_r and $\epsilon_0 = 1$ (air) the quasi static effective dielectric constant can be defined as

$$\epsilon_q = \frac{\epsilon_r + 1}{2}. \tag{2}$$

This quantity is just the arithmetic mean for the two half spaces. The phase velocity for a wave moving through this average dielectric is

$$V = \frac{c}{\sqrt{\epsilon_q}} \tag{3}$$

where c is the speed of light in vacuum.

The effective dielectric constant is frequency dependent and is given by [19]

$$\epsilon_{\text{eff}}(f) = \left[\sqrt{\epsilon_q} + \frac{\sqrt{\epsilon_r} - \sqrt{\epsilon_q}}{\left(1 + a\left(\frac{f}{f_{te}}\right)^{-b}\right)}\right]^2 \tag{4}$$

where a is

$$\log(a) \sim u \log\left(\frac{s}{w}\right) + v$$

and u and v depend on the substrate thickness, as:

$$u \sim 0.54 - 0.64q + 0.015q^2$$
$$v \sim 0.43 - 0.86q + 0.540q^2$$

and where $q = \log(s/h)$, and $b \sim 1.8$, are factors based on the line geometry [3], and f_{te} is

$$f_{te} = \frac{c}{4h\sqrt{\epsilon_r - 1}}. \tag{5}$$

The quantity f_{te} is the cutoff frequency above which a TE_1 surface wave begins to propagate. For the dimensions used in this work ($\epsilon_r = 13$, $h = 0.5$ mm) $f_{te} = 43$ GHz. Equation (4) is an approximation derived by curve fitting for the frequency dependence of a generalized conductor on a dielectric in an enclosed waveguide [19]. In the CAT line geometry it is not clear how to interpret (5) as the substrate is no longer uniform. For purposes of calculation it is assumed the substrate can be described by a uniform dielectric constant ϵ_r.

B. Attenuation

Conductor losses arise from finite metal conductivities σ. The resistance of a thick conductor at a given frequency, f is the same as the dc resistance of a conductor with (skin-effect) thickness, δ [20]

$$\delta = \frac{1}{\sqrt{f\mu\sigma\pi}} \tag{6}$$

where μ is the permeability and is assumed to be constant everywhere. The (characteristic) impedance Z_0 is given by [22]

$$Z_0 = \frac{120\pi}{\sqrt{\epsilon_{\text{eff}}}} \frac{K(k)}{K'(k)} \tag{7}$$

where $k = s/(s + w)$, s and w are the line dimensions shown in Fig. 1(b), and $K(k)$, $K'(k) = K(\sqrt{1 - k^2})$ are elliptic integrals. The ratio K/K' is [19]

$$\frac{K(k)}{K'(k)} = \frac{\pi}{\left\{\ln\left[2\frac{1 + \sqrt{k}}{1 - \sqrt{k}}\right]\right\}}; \quad \text{for } 0 \le k \le 0.707 \tag{7a}$$

$$\frac{K(k)}{K'(k)} = \frac{1}{\pi}\ln\left[2\frac{1 + \sqrt{k}}{1 - \sqrt{k}}\right]; \quad \text{for } 0.707 \le k \le 1.0. \tag{7b}$$

Note that Z_0 is frequency dependent since ϵ_{eff} is frequency dependent.

The frequency dependent surface impedance, Z_s is [21]

$$Z_s = \frac{(1 + j)}{\sigma\delta} \coth\left[(1 + j)\frac{t}{\delta}\right] \tag{8}$$

where j is the square root of minus one. Surface impedance is a complex quantity. This implies that in addition to attenuation (real part), there is a frequency dependent phase shift (imaginary part) due solely to the electrodes. In the limit of large t (thick electrodes) the coth term in (8) becomes unity.

The attenuation due to metal losses is [5]

$$\alpha_{\text{cond}}(f) = \text{Re}\left[\frac{Z_s(f)}{Z_0}\right] g \text{ dB/mm} \tag{9}$$

where g is a geometrical factor,

$$g = 17.34\left(\frac{P'}{\pi s}\right)\left(1 + \frac{w}{s}\right) \cdot \frac{\frac{1.25}{\pi}\ln\left[\frac{4\pi w}{t}\right] + 1 + \frac{1.25\,t}{\pi w}}{\left[1 + \frac{2w}{s} + \frac{1.25\,t}{\pi s}\left(1 + \ln\left[\frac{4\pi w}{t}\right]\right)\right]^2} \tag{9a}$$

and P' is

$$P' = \begin{cases} k[(1 - \sqrt{1 - k^2})(1 - k^2)^{3/4}]^{-1}\left[\frac{K(k)}{K'(k)}\right]^2; & \text{for } 0 \le k \le 0.707 \\ [(1 - k)\sqrt{k}]^{-1}; & \text{for } 0.707 \le k \le 1.0 \end{cases}. \tag{9b}$$

It is assumed that the electrode thickness is much greater than the mean free paths so that more complicated expressions that include the mean free path are not required for $\alpha_{\text{cond}}(f)$.

The attenuation due to radiation losses is given by [8]

$$\alpha_{\text{rad}}(f) = \pi^5 \frac{(3-\sqrt{8})}{2} \sqrt{\frac{\epsilon_{\text{eff}}(f)}{\epsilon_r}} \left(1 - \frac{\epsilon_{\text{eff}}(f)}{\epsilon_r}\right)^2 \cdot \frac{(s+2w)^2}{c^3 K'(k) K(k)} f^3. \tag{10}$$

Radiation losses arise from propagation speeds that exceed the speed of light in the higher dielectric substrate. As shown in [21], the energy lost in (10) goes into a Cherenkov half cone radiating into the substrate.

C. Dispersion

The dispersion characteristics of CPS's have been modeled by Hasnain *et al.* [3]. The phase due to the substrate is

$$\beta(f) = 2\pi \frac{f}{c} \sqrt{\epsilon_{\text{eff}}(f)}. \tag{11}$$

The metal electrodes result in an additional phase factor

$$\beta_{\text{cond}}(f) = \text{Im}\left[\frac{Z_s(f)}{Z_0}\right] g \text{ dB/mm}. \tag{12}$$

Both (11) and (12) contribute to the phase velocity

$$v_{ph}(f) = \frac{2\pi f}{\beta(f) + \beta_{\text{cond}}(f)}. \tag{13}$$

Depending on the design of the CPS, the electrode losses can have a significant influence. As line dimensions, and/or electrode thickness decrease, the electrode losses increase compared to the radiation losses.

The electrical input pulse for simulations is measured by electrooptic sampling as close to the excitation site as possible (<50 μm). For comparison with the cross-correlation measurement the calculated propagated pulse is convolved with the measured input pulse.

D. Small Geometries

In this section we consider the effect of small geometries on propagation. In this regime the electrode width w is comparable to the thickness t (i.e., the ratio $t/w = 0.04$–0.16). To correct for the finite electrode thickness a width Δ is added to the electrode spacing s, and subtracted from the width w [22]:

$$\Delta = \frac{1.25t}{\pi}\left[1 + \ln\left(\frac{4\pi w}{t}\right)\right] \tag{14}$$

i.e., $s = s_0 + \Delta$, and $w = w_0 - \Delta$.

In addition a thick electrode results in a larger amount of the electric field lines in the air between the conductors compared to a thin electrode and thus decreases the effective dielectric constant. A correction for ϵ_q (valid for $\epsilon_r \gtrsim 9$, $t/w < 0.1$) is also given in [22] as

$$\epsilon_q^t = \epsilon_q - \frac{1.4(\epsilon_q - 1)t/s}{K'(k)/K(k) + 1.4t/s} \tag{15}$$

where $K(k)$ and $K'(k)$ are elliptic integrals as in (7). These corrections are necessary to fit the measured propagation speed and attenuation.

IV. Simulation Results

The dependence of the total attenuation on the design parameters w and s for different frequencies is shown in Fig. 4. For very small dimensions, the total attenuation is dominated by electrode attenuation [skin-effect loss] (9) and at large dimensions by radiation (10). The minima in these curves indicate the optimum design parameters to transmit the desired frequency (e.g., 500 GHz) with the least loss. The pulses induced in the LT GaAs photoconductive switches are measured to be 0.8–1 ps FWHM and in the frequency domain the amplitude at 1 THz is about 10% of the dc value. In this case $w = s = 5$ μm is the appropriate design.

Fig. 5 shows the dependence of the total attenuation α_{tot} and the individual contributions radiation (α_{rad}) and conductor losses (α_{cond}) on w and s for a frequency of 500 GHz. This demonstrates that for values of $w = s$ below that for the minimum α_{tot}, conductor losses dominate and above, radiation losses dominate. A vertical line is shown at $w = s = 5$ μm. For this case the conductor losses are larger than the radiation losses, as opposed to [2] where $w = s = 50$ μm. The attenuation is plotted for two values of the substrate dielectric constant, 13.1 (GaAs substrate) and 2 (CAT line with an etched substrate). The value for CAT lines is obtained using (2) by comparing the propagation speed on a CAT loop with simulations.

In Fig. 6(a) the total attenuation as a function of frequency is shown for a conductor thickness of 0.2 μm and $\epsilon_r = 13.1$. The frequency ($f = 1.14$ THz) where $\alpha_{\text{rad}} = \alpha_{\text{cond}}$ is marked for $w = s = 5$ μm. Above this frequency radiation losses dominate over metal losses. This point shifts to lower frequencies for larger w and s. For a bandwidth of 500 GHz Fig. 6(a) shows a decrease in attenuation for w and s increasing from 1 to 5 μm. This decrease follows the increase in conductivity. For $w = s = 20$ μm, the attenuation at 500 GHz is larger than for $w = s = 1$ μm due to the large radiation component. At low frequencies where the skin depth exceeds the conductor thickness the conductor losses are determined by the bulk (dc) value of the conductivity. For thinner electrodes this results in increased absorption of low frequencies. On the loop structures these low frequencies appear as a background signal of a few GHz. Fig. 5(b) shows α_{tot} for $\epsilon_r = 2$; in this case α_{rad} is small (<0.2 mm^{-1} for 500 GHz as shown in Fig. 4) compared to α_{cond} over the entire range of conductor dimensions. At 500 GHz, the attenuation for an etched line with dimensions of ~ 20 μm are about ten times less than the *minimum* for an unetched line ($w = s$

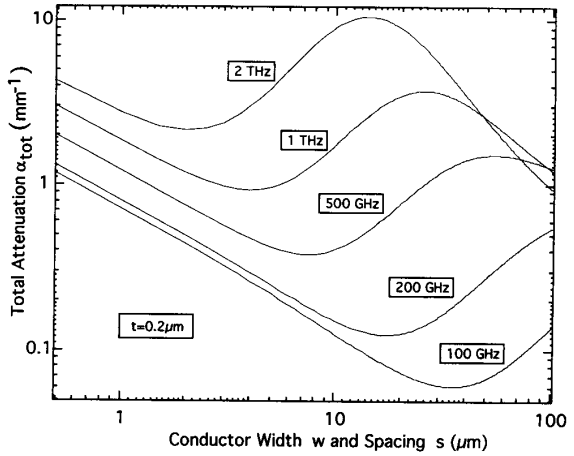

Fig. 4. Calculated dependence of total loss α_{tot} on design parameters w and s (for $w = s$) with a conductivity, $\sigma = 4.5 \times 10^7\ \Omega^{-1} \cdot m^{-1}$ and a thickness, $t = 0.2\ \mu m$.

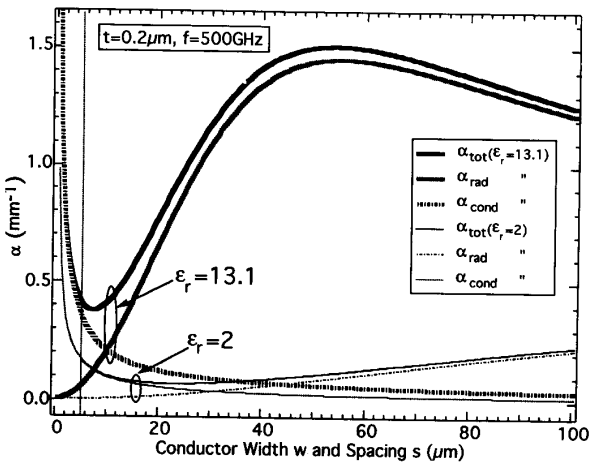

Fig. 5. Calculated contributions of conductor and radiation losses to the total loss α_{tot} for $\epsilon_r = 2.0$ (CAT lines) and 13.1 (CPS lines) at a frequency of 500 GHz. The vertical dotted line corresponds to line dimensions of $w = s = 5\ \mu m$. For the example shown the CAT line is expected to have a factor of two improvement in *attenuation* for the same electrode configuration as a CPS line.

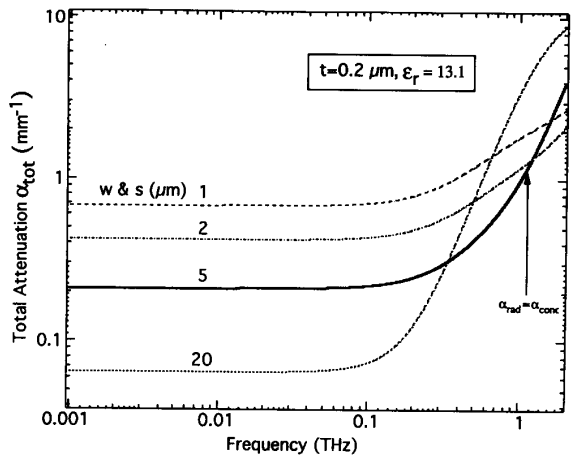

(a)

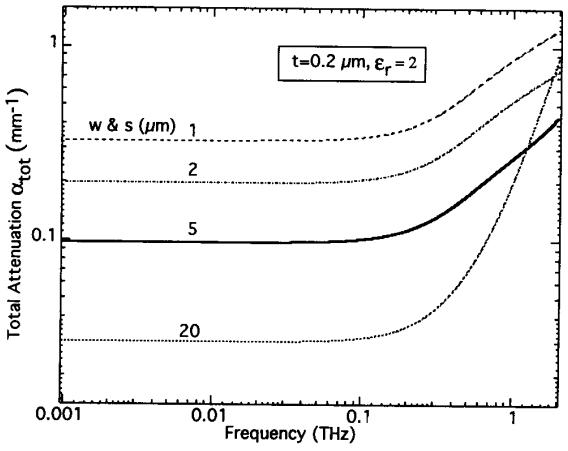

(b)

Fig. 6. (a) Calculated frequency dependence of the total attenuation of CPS lines. $\alpha_{rad} = \alpha_{cond}$ indicates the frequency (1.14 THz) above which the radiation losses become dominate for dimensions $w = s = 5\ \mu m$ and thickness of 0.2 μm. (b) Frequency dependence of the total attenuation for CAT lines with the same dimensions as (a).

$= 5\ \mu m$). This reduction is mainly due to the reduction in the radiative component, as shown in Fig. 5.

Another important feature for signal transmission with small distortion is a small variation in (11) and (12) or the phase velocity v_{ph} over the whole frequency range, i.e., low dispersion. The results of calculations are shown for $\epsilon_r = 13.1$ [Fig. 7(a)] and for $\epsilon_r = 2$ [Fig. 7(b), note that the scale is extended compared to Fig. 7(a)]. For unetched lines the 5 μm line shows the best result with v_{ph} being almost constant from dc to 2 THz. From Fig. 7(a) we see that 20 μm lines will produce significant dispersion at 500 GHz, in addition to increased attenuation at high frequencies. In CAT lines [Fig. 7(b)] this performance is improved, dispersion is significantly less and electrode dimensions are not as critical as for the CPS line. The CAT line velocity is twice as fast as the unetched line. Note that in both Fig. 7(a) and 7(b) it should be possible to choose a geometry (for a given set of etch conditions and electrode thickness) such that v_{ph} is essentially flat (i.e., the absolute value of $[v_{max} - v_{min}] < 1\%$) with respect to frequency from dc to beyond 1 THz.

V. Gold Electrodes at Low Temperatures

Normal metal electrodes will improve their resistivity at lower temperature according to Mathiessen's rule [23]:

$$\rho(T) = \rho_1(T) + \rho_0 \tag{16}$$

where $\rho_1(T)$ is the temperature dependent resistance due to inelastic processes such as electron-phonon interaction

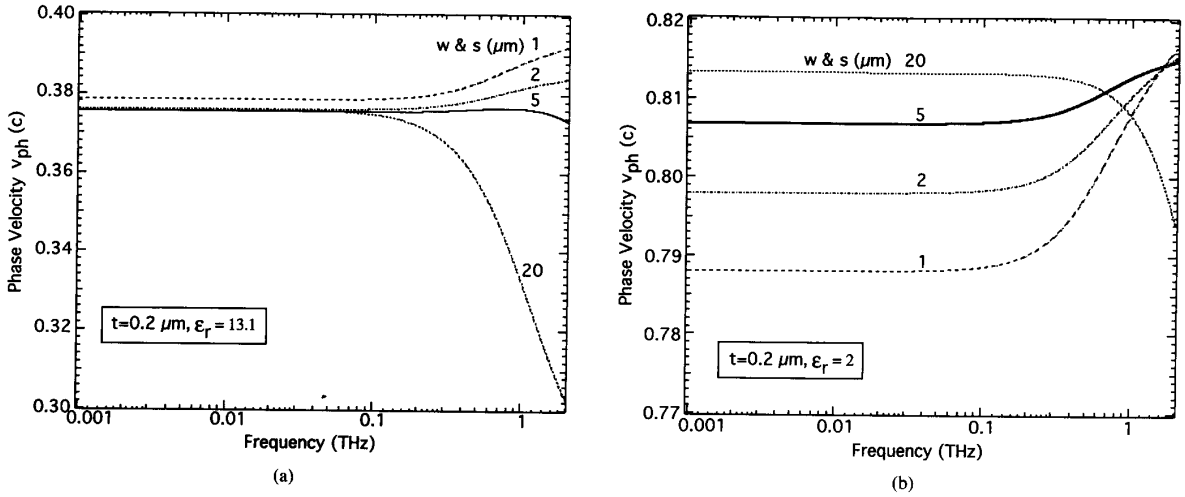

Fig. 7. (a) Calculated phase velocity, v_{ph} for CPS lines (ϵ_r = 13.1) and (b) CAT lines (ϵ_r = 2.0).

TABLE I
MEASURED AND FITTED PARAMETERS OF THE THIN FILMS USED. RESISTIVITIES ARE FOUR WIRE MEASUREMENTS MADE ON A 3.45 mm LONG TRANSMISSION LINE

Electrode Thickness (μm)	ρ (295 K) (μΩ cm)	ρ (2 K) (μΩ cm)	R 295 K (Ω)	R 2 K (Ω)	σ_{dc} (295 K) ($10^7\ \Omega^{-1}\ m^{-1}$)	σ_{dc} (2 K) ($10^7\ \Omega^{-1}\ m^{-1}$)	σ_{fit} (295 K) ($10^7\ \Omega^{-1}\ m^{-1}$)	σ_{fit} (2 K) ($10^7\ \Omega^{-1}\ m^{-1}$)	RRR
1.2 (Ge-Pd-Au)	2.7	0.18	15.37	1.05	3.7	56	2.1	56	14.6
0.37 (Ti-Au)	3.3	0.56	60.9	10.3	3.0	18	1.6	3	
0.24 (Au)	3.4	0.70	97.6	19.9	3.0	15	1.4	3	
0.2 (Ge-Pd-Au)	4.7	2.1	161.9	72.7	2.1	4.8	1.23	2.75	

in the material, and ρ_0 is the temperature independent contribution to resistance. The ρ_0 portion includes scattering due to crystal imperfections, film granularity, surfaces or edges, etc. The resistivity of a thin film decreases with decreasing temperature and reaches a minimum value limited by ρ_0. A given thin film may be characterized by the residual resistivity ratio (RRR) which we define as the ratio of the resistivity at room temperature (T = 295 K) to the low temperature (T = 2 K) resistivity. The results for the films used in this work are shown in Table I and are all four-wire resistance measurements made on a fabricated transmission line.

VI. ELECTRODE MEASUREMENTS

Electrode effects were studied by pulse propagation measured on a CPS loop 1 mm in diameter. This made measurements of many round-trips possible, up to 6 cm total propagation distance.

In order to verify the negligible effect of the transmission line curvature, measurements were made on identically prepared straight transmission lines as well as loops 0.5 mm in diameter. No measurable deviation is found for any of the designs tested. Note that the ratio of line width to loop diameter is 5×10^{-3} for the 1 mm loop.

Measurements were performed over a range of temperatures from 2 to 300 K and for electrode thicknesses from 0.2 to 1.2 μm. Fig. 8 shows a direct comparison of measurement and simulation for t = 1.2 μm at T = 295 K. The first and second peak correspond to an optical beam separation and electrical propagation distance of 0.5 mm. The simulation is normalized to the amplitude of the second peak. Small reflections seen around 50 ps are likely to be due to the perpendicular bias lines [Fig. 1(a)]. Compared to the measurement at T = 2 K the attenuation is much stronger and is fitted with a conductivity $\sigma_{fit} = 2.1 \times 10^7\ \Omega^{-1}m^{-1}$ which is less than the measured dc value (Table I). For 2 K, however, the dc value ($5.6 \times 10^8\ \Omega^{-1}m^{-1}$) gives a perfect fit with respect to the measured attenuation. In order to simulate the propagation speed it is important to take into account the correction of ϵ_{eff} for finite electrode thickness (14). The fit is very sensitive to changes in ϵ_r and the error due to fitting the measured propagation speed is less than 0.2. This correction is equivalent to assuming an ϵ_r = 10.5. The thick electrodes increase the propagation speed considerably, as the taller profile causes more of the electric field to be out of the higher dielectric substrate. Fig. 9(a) shows measurements made at different temperature for a thin (t = 0.2 μm) electrode. Comparing the room temperature measurement with Fig. 8 shows the attenuation is much stronger with negligible amplitude after the second round-trip. The com-

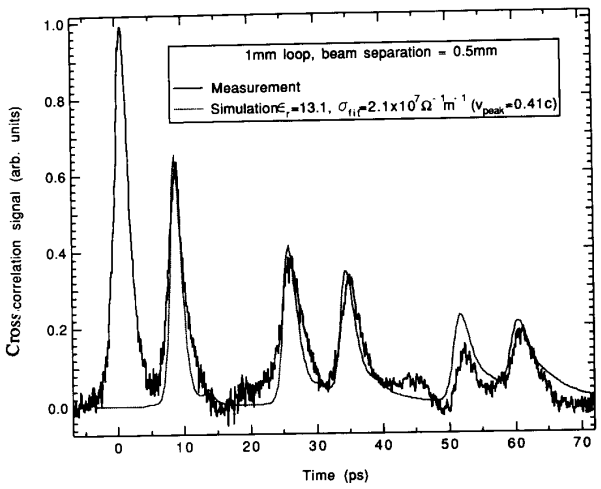

Fig. 8. Comparison of cross-correlation measurement and simulation.

parison of measurements at different temperatures reveals the influence of the conductivity on attenuation. The measured dc values σ_{dc} are given in the graph. The simulations of these measurements are shown in Fig. 9(b). In contrast to the previously discussed simulations for thick electrodes, here the best results (in terms of matching the propagation speed) are obtained by using the thin electrode approximation and not using the thickness correction for ϵ_r (15). If the absolute delay is not measured, the velocity error incurred by using (15) would go unnoticed. While no lower limit for (15) is listed in [22], 200 nm is found to be a lower bound. The conductivities chosen to fit the calculated amplitudes to the measurements are about a factor of two smaller than the dc values, but scale with temperature by the same amount. A possible explanation for this deviation is that the high frequency (skin effect) conductivity near the surface is less than the average value measured at dc. For high frequencies the small skin depth will dominate the attenuation as shown in Fig. 4. The underestimation of the attenuation by using σ_{dc} in the calculation rather than σ_{fit} is seen for all samples. These results are summarized in Table I.

VII. CAT Line Measurement

As shown in (3) the velocity of propagation varies inversely with the square root of the effective dielectric constant. Clearly, removing the substrate dielectric in and around the electrodes is will reduce ϵ_q and so increase the propagation velocity. As shown in Fig. 10 large velocities can be obtained by deep etching ("Glass Cat": $v = 0.86$) or by reducing the supporting SiO_2 layer to a series of supports running perpendicular to the electrodes like telephone poles so that the electrodes are essentially free-standing ("Free CAT": $v = 0.9c$). As expected, an unetched sample has a velocity of $0.39c$ ("GaAs no etch" in Fig. 10).

For comparison to simulations, a propagation speed (of the pulse peak) of $0.81c$ for a CPS on a uniform substrate

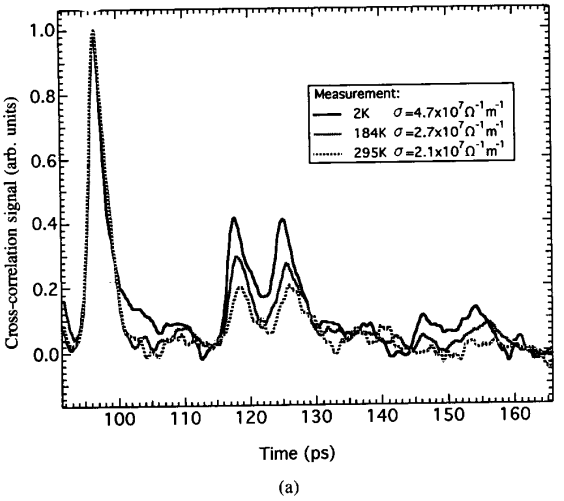

(a)

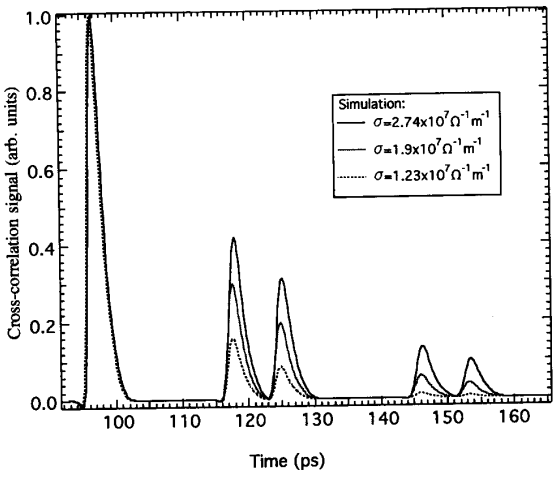

(b)

Fig. 9. (a) Cross-correlation measurement on a CPS loop with $t = 0.2\ \mu$m for different temperatures. (b) Simulations with electrode conductivity, σ_{fit} as the fitted parameter.

would require a dielectric constant of $\epsilon_r = 2.0$. This is the value measured on a 1 mm CAT loop and is used in Figs. 5, 6(b), and 7(b). It indicates that for the CAT lines the substrate still has some influence on pulse propagation. Attenuation and dispersion, however, could not be accurately measured in this design as the measurements showed significant additional losses due to energy propagating into the contact pads. The particular etch mask used in this work allowed only a single pump and probe location, adjacent to the bias lines. After etching the photoconductive island and bias lines remain intact, presenting a better impedance match than the (etched) transmission line. In contrast to this loop, a straight CAT line exhibited a propagation speed of only $0.61c$ (corresponding to $\epsilon_r = 5.2$) indicating that this particular line was not etched as deeply. In addition to an improvement in speed we expect an improvement in attenuation. From (9) it is

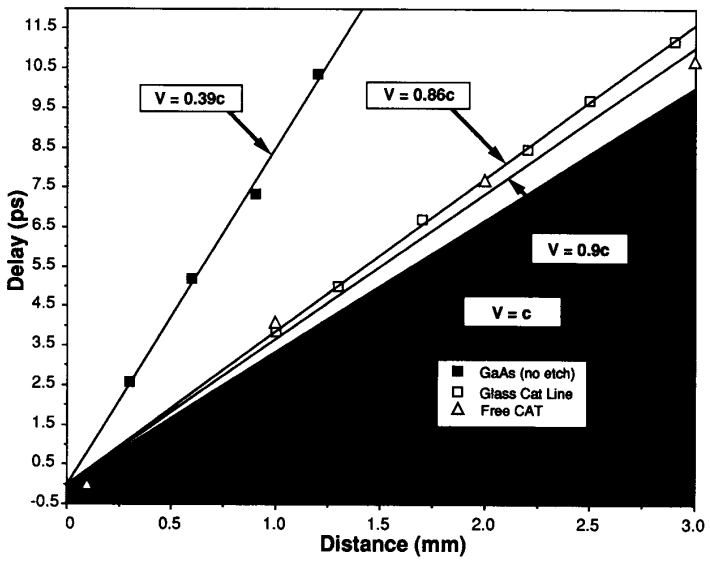

Fig. 10. Plot of delay (as measured by midpoint of linear fit to risetime) versus propagation distance. Glass CAT corresponds to the geometry of Fig. 2 and Free CAT corresponds to the periodically supported telephone pole arrangement. Velocity v is found from a linear fit to the data. Shaded area is bordered by $v = c$.

evident that β, the phase factor decreases as the square root of the effective dielectric constant. However, from (6) we see that the electrode attenuation also scales (through the characteristic impedance) as the square root of the effective dielectric constant. The attenuation for the CAT line ($\alpha = 0.16\ \text{mm}^{-1}$) is about *half* of the attenuation for the equivalent CPS structure ($\alpha = 0.26\ \text{mm}^{-1}$). Fig. 11 shows the measured and simulated signal at a distance of 1.0 and 3.0 mm. The structure in the signal (after the main pulse) at 1.0 mm is due to a reflection caused at the launch site of the pulse. There is only a small distance between the large contact pads ($100 \times 100\ \mu$m) and the photoconductive switch which presumably causes the reflections. The same situation exists at the far end of the line. This was verified by electrooptic sampling of the signal at the photoconductive switch and following the waveform as it propagates down the line while maintaining its basic shape.

In order to measure the risetime, the optical fiber was removed to prevent dispersion of the fs excitation pulse. A summary of risetime measurements versus distance from 100 μm to 2.8 mm is given in Fig. 12. Note that the measured rise time is only 0.8 ps and 2.8 mm of propagation. The zero distance intercept of 370 fs gives a measure of the overall system response, for this configuration, which includes the effects of the sampling crystal, velocity mismatch between the electric and optical waves inside the $LiTaO_3$, etc.

A summary of the measured data for etched and unetched samples is shown in Fig. 13. With the exception of the very thick (1.2 μm) electrodes, the reduction in high-frequency attenuation for the CPS line as a function of temperature scales as the reduction in the dc conductivity. The data from Fig. 11 is shown as the filled circle in Fig. 13.

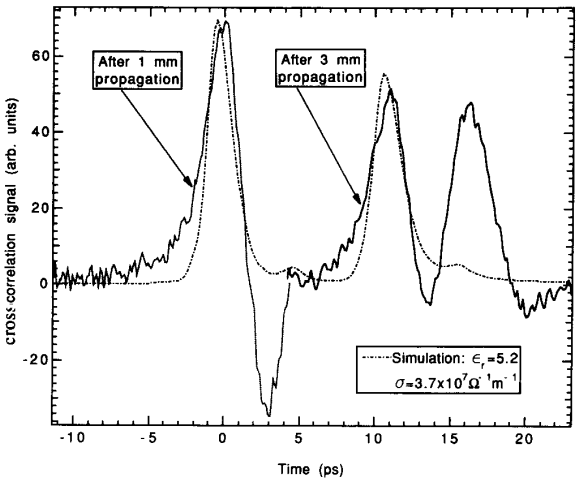

Fig. 11. Measured and calculated cross correlation for a straight CAT line at propagation distances of 1.0 and 3.0 mm. The time axis has been shifted so that $t = 0$ occurs at the peak of the pulse at 1 mm. The corresponding simulation shown uses the dc value for σ, and ϵ_r is chosen to match the propagation speed. The reflections in the waveforms are due to contact pads at each end of the line.

VIII. Energy Considerations

In addition to high fidelity long distance propagation, CAT lines also result in reduced charging energies compared to unetched transmission lines. If we model the transmission line electrodes as cylinders of diameter d separated by a center to center distance s_c then the characteristic impedance Z_0 in a uniform dielectric is given by

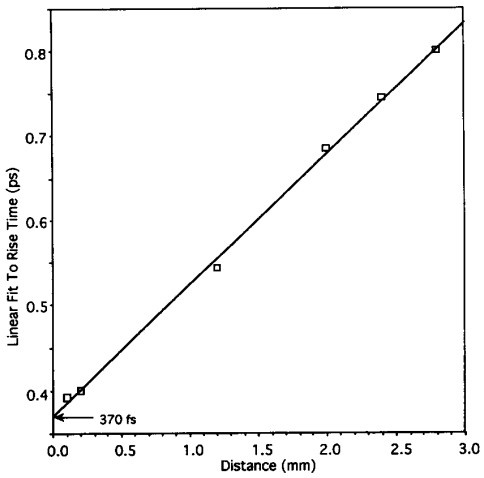

Fig. 12. Plot of rise time (as measured by midpoint of linear fit to rise time) versus propagation distance. The zero distance intercept gives a system response rise time of 370 fs. Measured rise time after 2.8 mm of propagation is 0.8 ps.

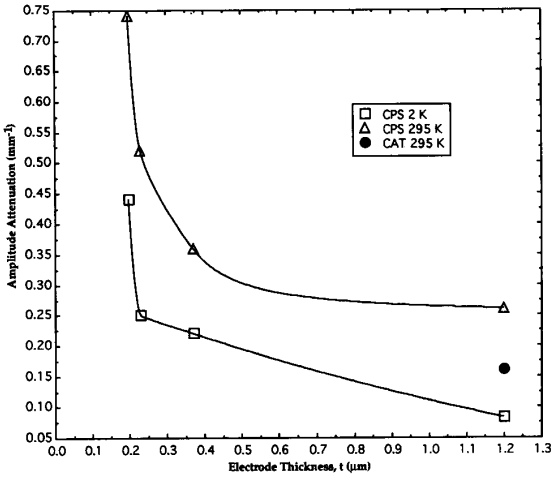

Fig. 13. Measured attenuation versus conductor thicknesses at 2 *K* and 295 *K*. Curves are guides to the eye. The 1.2 μm thick CAT line shows a factor of two improvement in *attenuation* for the identical electrode configuration (thickness, width and spacing) as a CPS line.

[20]

$$Z_0 = \frac{\eta}{\pi} \cosh^{-1}\left[\frac{s_c}{d}\right] \tag{17}$$

where the intrinsic impedance is $\eta = \sqrt{\mu_0/(\epsilon_q\epsilon_0)}$ and $\sqrt{\mu_0/\epsilon_0} = 377\ \Omega$ (in Fig. 1, $w = s_c - d$). Using the average value of $\epsilon_r = 6.92$ for the dielectric of the unetched line with $s_c = 10\ \mu$m and $d = 5\ \mu$m, (17) yields $Z_0 = 60\ \Omega$. The characteristic impedance for the CAT line is *increased* by a factor of more than 2.2 to 136 Ω since Z_0 scales as $1/\sqrt{\epsilon_q}$. Thus, a CAT line with the measured ϵ_r of 1.35, but with $d = 2\ \mu$m and $s_c = 2.24\ \mu$m has an impedance of $\sim 50\ \Omega$.

Using the same model [20] of two cylindrical conductors in a uniform dielectric, the capacitance C is

$$C = \frac{\pi\epsilon_0\epsilon_q}{\cosh^{-1}\left[\frac{s_c}{d}\right]}. \tag{18}$$

The capacitance scales as the dielectric constant, ϵ_q and so is reduced by 4.8 times in the etched line to 28.5 fF/mm. For a line resistivity of 2 $\mu\Omega \cdot$ cm with 1×5 μm lines the characteristic RC time constant is 1.1 ps for a 1 mm long line (for a digital circuit, the entire line is driven).

The energy required to charge the line $\frac{1}{2}CV^2$ scales as ϵ_q and so is reduced by a factor of 4.8. For a load resistor R matched to Z_0 the energy dissipated is $\frac{1}{2}V^2/R$ and scales as $1/\sqrt{\epsilon_q}$, so the total energy required to drive the CAT line is reduced by a factor of more than 7 (4.8 from the reduction in C plus a little more than 2.2 from the reduction in the required load resistor) compared to the unetched case.

IX. Summary

In this paper we have demonstrated a new technique for the study of ultrafast signal propagation, loop transmission lines. The loop configuration allows long distance (≤ 6 cm) propagation studies to be made in a small area. This in turn allows measurements to be made at low temperatures. The loop configuration yields not only velocity, but amplitude and phase information, which is necessary for accurate modeling of signal propagation. Careful characterization of the electrodes is also required for accurate modeling of the measured results.

The measured signals are modeled considering only electrode absorption and radiation loss. Equations based largely on approximations for other geometries are shown to yield good results for amplitude and phase. By measuring electrodes of different thickness as a function of temperature, an accurate comparison can be made of the dispersion characteristics, as well as the speed of a given transmission line.

In addition, the effects of substrate removal are shown to influence not only the speed of a given transmission line, but also the attenuation, through lowering of the surface impedance. We show that at 500 GHz, CAT lines can be designed with ten times less attenuation than the optimal (i.e., lowest total attenuation) unetched case. For equivalent dimensions the attenuation in CAT lines is measured to be about half that of an unetched line. A simple energy analysis, based on a uniform dielectric, shows a seven times reduction in the energy required to charge a CAT line.

In real chips, corners, as well as straight lines are required. We have demonstrated that bends of radius 0.25 mm are capable of high-fidelity signal transmission. As an alternative to using bends (which occupy significant chip area) active devices can be used to redirect a pulse at right angles to the input pulse. Our results suggest that digital, intrachip communication on length scales of order

1 cm with pulses as short as one picosecond and velocities as high as $0.8c$ is readily achievable using electrical signals.

ACKNOWLEDGMENT

We acknowledge helpful discussions with N. Zimmerman, I. N. Duling III, and M. Y. Frankel, all of N.R.L.

REFERENCES

[1] J. Hauenschild, H. -M. Rein, W. McFarland, and D. Pettengill, "24 Gbit/s regenerating demultiplexer IC in silicon bipolar technology," *Electron. Lett.*, vol. 27, no. 6, p. 502.

[2] D. A. B. Miller, "Optics for low-energy communication inside digital processors: Quantum detectors, sources, and modulators as efficient impedance converters," Lett., 14, p. 146, 1989, and M. R. Feldman, S. C. Esener, C. C. Guest, and C. H. Lee, "Comparison between optical and electrical interconnects based on power and speed considerations," *Appl. Opt.*, vol. 27, p. 1742, 1988.

[3] G. Hasnain, A. Dienes, and J. R. Whinnery, "Dispersion of picosecond pulses in coplanar transmission lines," *IEEE Trans. Microwave Theory Technol.*, vol. MTT-34, p. 738, 1986.

[4] J. F. Whitaker, R. Sobolewski, D. R. Dykaar, T. Y. Hsiang, and G. A. Mourou, "A propagation model for ultrafast signals on superconducting dispersive striplines," *IEEE Trans. Microwave Theory Technol.*, vol. 36, p. 277, Feb. 1988.

[5] W. J. Gallagher, C.-C. Chi, I. N. Duling III, D. Grischkowsky, N. J. Halas, M. B. Ketchen, and A. W. Kleinsasser, "Subpicosecond optoelectronic study of resistive and superconductive transmission lines," *Appl. Phys. Lett.*, vol. 50, p. 350, 1987.

[6] D. S. Phatak and A. P. Defonzo, "Dispersion characteristics of optically excited coplanar striplines: Pulse propagation," *IEEE Trans. Microwave Theory Technol.*, vol. 38, p. 654, May 1990.

[7] M. C. Nuss, and K. W. Goossen, "Investigation of high-temperature superconductors with terahertz bandwidth electrical pulses," *IEEE J. Quantum Electron.*, vol. 25, p. 2596, 1989.

[8] M. Y. Frankel, S. Gupta, J. A. Valdmanis, and G. A. Mourou, "Terahertz attenuation and dispersion characteristics of coplanar transmission lines," *IEEE Trans. Microwave Theory Technol.*, vol. 39, p. 910, June 1991.

[9] J. Ness, S. Williamson, and G. A. Mourou, "100 GHz travelling-wave electro-optic modulator," *Appl. Phys. Lett.*, vol. 54, no. 20, p. 1962, 1989.

[10] D. R. Dykaar, A. F. J. Levi, and M. Anzlowar, "Ultrafast coplanar-air transmission lines," *Appl. Phys. Lett.*, vol. 57, no. 11, p. 1123, 1990.

[11] W. H. Knox, J. E. Henry, K. W. Goossen, K. D. Lee, B. Tell, D. A. B. Miller, D. S. Chemla, A. C. Gossard, J. English, and S. Schmitt-Rink, "Femtosecond excitonic optoelectronics," *IEEE J. Quantum Electron.*, vol. 25, p. 2586, Dec. 1989.

[12] F. W. Smith, H. Q. Lee, V. Diadiuk, M. A. Hollis, A. R. Calawa, S. Gupta, M. Frankel, D. R. Dykaar, G. A. Mourou, and T. Y. Hsiang, "Picosecond GaAs-based photoconductive optoelectronic detectors," *Appl. Phys. Lett.*, vol. 54, no. 10, p. 890, 1989.

[13] D. R. Dykaar, D. J. Eaglesham, U. D. Keil, B. J. Greene, P. N. Saeta, L. N. Pfeiffer, R. F. Kopf, S. B. Darack, and K. W. West, "Molecular beam epitaxy of low temperature grown GaAs photoconductors," *MRS Proc.*, vol. 241, to be published.

[14] D. R. Dykaar, T. Y. Hsiang, and G. A. Mourou, "Development of a picosecond cryo-sampler," *Topical Meeting on Picosecond Electronics and Optoelectronics*, New York: Springer-Verlag, 1985, p. 249.

[15] M. B. Ketchen, D. Grischkowski, T. C. Chen, C.-C. Chi, I. N. Duling III, N. J. Halas, and J. M. Halbout, "Generation of subpicosecond electrical pulses on coplanar transmission lines," *Appl. Phys. Lett.*, vol. 48, p. 751, 1986.

[16] J. A. Valdmanis, R. L. Fork, and J. P. Gordon, "Design considerations for a femtosecond pulse laser balancing self-phase modulation, group velocity dispersion, saturable absorption, and saturable gain," *IEEE J. Quantum Electron.*, vol. QE-22, p. 112, 1986.

[17] J. A. Valdmanis and G. A. Mourou, "Subpicosecond electrooptic sampling: Principles and applications," *IEEE J. Quantum Electron.*, vol. QE-22, p. 69, 1986, and J. M. Chwalek and D. R. Dykaar, "A mixer based electro-optic sampling system for sub-millivolt signal detection," *Rev. Sci. Instrum.*, vol. 61, p. 1273, Apr. 1990.

[18] D. H. Auston, in *Picosecond Optoelectronic Devices*, C. H. Lee, Ed. New York: Academic, 1984, pp. 73-116.

[19] E. Yamashita, K. Atsuki, and T. Ueda, "An approximate dispersion formula of microstrip lines for computer-aided design of microwave integrated circuits," *IEEE Trans. Microwave Theory Technol.*, vol. 27, p. 1036, Dec. 1979.

[20] S. Ramo, J. R. Whinnery, and T. Van Duzer, *Fields and Waves in Communication Electronics*, New York: Wiley, 1965.

[21] D. B. Rutledge, D. P. Neikirk, and D. P. Kasilingham, in *Infrared and Millimeter Waves*, K. J. Button, Ed. New York: Academic, vol. 10, pt. 2, 1983.

[22] K. C. Gupta, R. Garg, and I. J. Bahl, *Microstrip Lines and Slotlines*, Dedham, MA: Artech House, 1970, 1979.

[23] L. I. Maissel, *Handbook of Thin Film Technology*, New York: McGraw-Hill, p. 13-1.

Ulrich D. Keil was born in Düsseldorf, Germany, on October 16, 1960. He attended the University of Düsseldorf and the University of Bielefeld where he received the Dipl.Phys. degree in 1985. In 1987 he joined the Institut für Technische Physik, Erlangen, where he received the Dr.rer.nat. degree in 1990 with a dissertation about photoreflectance of doping superlattices.

From 1986 to 1987 he worked in the Excimer Laser Development Group for Siemens/KWU, Erlangen, Germany. Since 1991 he has been a post-Doctoral Fellow at AT&T Bell Laboratories, Murray Hill, NJ, where his research interest is ultrafast spectroscopy of semiconductor devices.

Douglas R. Dykaar (S'80-M'86-S'86-M'87), for a photograph and biography, see this issue, p. 2312.

A. F. J. Levi, photograph and biography not available at the time of publication.

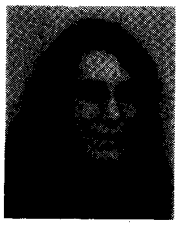

Rose F. Kopf received the B.Sc. degree in chemistry from Northeastern University, Boston, MA, in 1982 and the M.S. and Ph.D. degrees in materials science and engineering in 1987 and 1991, respectively, both from Stevens Institute of Technology, Hoboken, NJ. While in school for the B.Sc. degree, she worked at A. D. Little, Inc., Cambridge, MA, as an analytical chemist.

From 1982 to 1984, she worked for Crystal Diagnostics Systems, Inc., Woburn, MA, also as an analytical chemist. Since she joined AT&T Bell Laboratories in 1984, she has been involved in the MBE growth of GaAs-AlGaAs and AlInAs-GaInAs, lattice-matched to InP, heterostructures. Some of this work includes FET, HBT, QWIP, VCSEL and SEED structures. Additionally, she has written software for the MBE computer control system for the growth of compositionally graded structures in both material systems. She has over 100 publications and holds several patents.

L. N. Pfeiffer, photograph and biography not available at the time of publication.

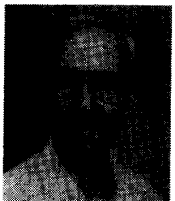

Sheldon B. Darack was born in Hartford, CT. He received the B.A. degree from Yeshiva University, New York, NY, in 1968 and the M.S. degree in physics from Stevens Institute of Technology, Hoboken, NJ, in 1975.

He has been with AT&T Bell Laboratories since 1970. He has worked on low temperature magnetic susceptibility studies of rare-earth intermetallic compounds, RF plasma grown oxides of semiconductors, and currently, ultrashort pulse lasers.

K. W. West, photograph and biography not available at the time of publication.